



A Collection of New Dwarf Galaxies in NGC 5128's Western Halo

Matthew A. Taylor¹, Paul Eigenthaler², Thomas H. Puzia², Roberto P. Muñoz²,
Karen X. Ribbeck², Hong-Xin Zhang³, Yasna Ordenes-Briceño², and Mia Sauda Bovill⁴

¹Gemini Observatory, Northern Operations Center, 670 North A'ohoku Place, Hilo, HI 96720-1906, USA; mtaylor@gemini.edu

²Instituto de Astrofísica, Pontificia Universidad Católica de Chile, Av. Vicuña Mackenna 4860, 7820436 Macul, Santiago, Chile

³CAS Key Laboratory for Research in Galaxies and Cosmology, Department of Astronomy,

University of Science and Technology of China, Hefei 230026, People's Republic of China

⁴Texas Christian University, Dept. of Physics and Astronomy, 2800 South University Drive, Fort Worth, TX 76129, USA

Received 2018 August 16; revised 2018 October 14; accepted 2018 October 15; published 2018 October 30

Abstract

We report the photometric properties of 16 dwarf galaxies, 15 of which are newly identified, in the Western halo of the nearby giant elliptical galaxy NGC 5128. All of the candidates are found at projected distances $\sim 100\text{--}225$ kpc from their giant host, with luminosities $-10.82 \leq M_V/\text{mag} \leq -7.42$ and effective radii $4'' \lesssim r_{\text{eff}} \lesssim 17''$ (or $75 \lesssim r_{\text{eff}}/\text{pc} \lesssim 300$ at the distance of NGC 5128). We compare them to other low-mass dwarf galaxies in the local universe and find that they populate the faint/compact extension of the size–luminosity relation that was previously not well-sampled by dwarf galaxies in the Centaurus A system, with optical colors similar to compact stellar systems like globular clusters and ultra-compact dwarf galaxies despite having much more diffuse morphologies. From optical $u'g'r'i'z'$ photometry, stellar masses are estimated to be $5.17 \leq \log M_*/M_\odot \leq 6.48$, with colors that show them to fall redward of the dwarf galaxy mass–metallicity relation. These colors suggest star formation histories that require some mechanism that would give rise to extra metal enrichment such as primordial formation within the halos of their giant galaxy hosts, non-primordial star formation from previously enriched gas, or extended periods of star formation leading to self-enrichment. We also report the existence of at least two subgroups of dwarf candidates, each subtending $\lesssim 15'$ on the sky, corresponding to projected physical separations of 10–20 kpc. True physical associations of these groups, combined with their potentially extended star formation histories, would imply that they may represent dwarf galaxy groups in the early stage of interaction upon infall into a giant elliptical galaxy halo in the very nearby universe.

Key words: galaxies: dwarf – galaxies: elliptical and lenticular, cD – galaxies: individual (NGC 5128)

1. Introduction

A renaissance is underway regarding the discovery rate of low-luminosity dwarf galaxies throughout the local universe at distances $\lesssim 50$ Mpc. The known population of dwarf galaxies in the Local Group (LG) has risen in the last decade to include dozens (e.g., Belokurov et al. 2010; McConnachie 2012; Bechtol et al. 2015; Muñoz et al. 2018a, 2018b), while rich dwarf galaxy systems beyond the LG have been discovered in myriad environments including galaxy clusters like Virgo and Fornax (Muñoz et al. 2015; Sánchez-Janssen et al. 2016; Eigenthaler et al. 2018; Ordenes-Briceño et al. 2018a) and smaller complexes including M81, M101, NGC 2784, M96, and others (e.g., Chiboucas et al. 2009; Merritt et al. 2014; Javanmardi et al. 2016; Bennet et al. 2017; Henkel et al. 2017; Müller et al. 2017b, 2018a; Park et al. 2017; Smercina et al. 2017). It becomes increasingly apparent that such dwarf galaxy systems exhibit seemingly structured distributions around their host gravitational potentials, with surprisingly thin, planar distributions found around the LG (Ibata et al. 2013; Pawlowski et al. 2012), and evidence for sub-100 kpc scale clustering for dwarfs orbiting within the half-virial sphere of the Fornax galaxy cluster (Muñoz et al. 2015; Ordenes-Briceño et al. 2018a).

The nearby giant elliptical galaxy NGC 5128 has proven to be no exception to the above findings. Recent years have seen the discovery of several new dwarf galaxy satellites, including the existence of a co-rotating plane of satellites surrounding NGC 5128 itself (Müller et al. 2018b) and numerous dwarf galaxies among tidal debris in NGC 5128's northeastern halo

(Crnojević et al. 2014, 2016). This is all part of an apparent “bridge” of satellites spread northward from NGC 5128, toward the associated giant galaxy M83 (Müller et al. 2015, 2016, 2017a). Meanwhile, the globular cluster (GC) system of NGC 5128 has been found to extend in the 1000s to at least 200 kpc—and very likely beyond—which is dominated by blue, presumably metal-poor, GCs (Taylor et al. 2017). The existence of such a rich population of blue GCs may suggest the existence of a former and/or present reservoir of low-mass dwarf galaxy GC hosts. Given the above, there is a natural motivation to search for yet more dwarf galaxies in NGC 5128's halo, particularly in the northern regions where higher numbers of dwarfs might be expected to accompany the NGC 5128-M83 bridge.

We focus in this Letter on a region $\sim 100\text{--}225$ kpc into the northwestern halo, where sparse deep imaging data has been obtained to date. In what follows we report the properties of 16 dwarf galaxy candidates (15 of which are new). We determine multi-band luminosities and structural parameters that are used to broadly compare to other low-mass systems throughout the local universe and to predictions of simple stellar population (SSP) evolutionary model tracks. Throughout this Letter, we adopt a NGC 5128 distance modulus of 27.88 mag (3.8 Mpc Harris et al. 2010), corresponding to a spatial scale of $19 \text{ pc arcsec}^{-1}$.

2. Observations and Image Processing

Observations in the optical $u'g'r'i'z'$ filters were obtained as part of the Survey of Centaurus A's Baryonic Structures

campaign (Taylor et al. 2017) that uses the Dark Energy Camera (DECam) mounted on the 4 m Blanco telescope at the Cerro Tololo Interamerican Observatory (CTIO) to image ~ 72 deg² of the sky around NGC 5128. Specifically, for each filter we utilize a set of DECam images centered on $(\alpha, \delta) = (13: 16: 30.83, -42: 21: 41.06)$. Images were acquired over 2014 April 4–5 with total integration times of 1200, 100, 60, 100, and 200 s targeted to reach a signal-to-noise ratio (S/N) \approx five point-source depths of 24.1, 22.7, 22.5, 22.1, and 21.7 in the u' , g' , r' , i' , and z' filters, respectively. Image preprocessing was carried out by the DECam community pipeline (CP; Valdes et al. 2014) to remove instrumental signatures (bias subtraction, flat-fielding, cross-talk correction, fringing, etc.). From the CP calibrated frames, we use the ASTROMATIC⁵ software suite (Source Extractor (SE); SCAMP; SWARP; PSFEX; Bertin & Arnouts 1996; Bertin et al. 2002; Bertin 2006) to register frames to a common coordinate system and account for pixel scale distortions across the DECam field of view using the 2MASS astrometric reference star catalog and calibrate our photometry to the Sloan Digital Sky Survey (SDSS) system using frames of the LSE_44 SDSS southern standard star field taken at varying airmass during the observing nights.

3. Analysis

3.1. Dwarf Detection and Photometric Analysis

We detect dwarf candidates using a full-color RGB image constructed from our $u'g'z'$ imaging with custom PYTHON image processing scripts. This filter combination samples the full optical spectral energy distribution (SED) and is sensitive to old, metal-poor stellar populations expected of primordial dwarf galaxies, while the inclusion of the u' -band also serves to sample flux from younger stellar components arising from more recent star formation. Figure 1 shows the RGB image with orange dashed curves indicating NGC 5128-centric iso-radial contours. We visually searched this image for faint, extended sources displaying smooth morphologies with shallow surface-brightness (μ) profiles typical of low-luminosity dwarfs. Using this method, we unambiguously find 16 dwarf galaxy candidates, of which a single previously known dwarf is recovered (KK98a 189; Karachentseva & Karachentsev 1998) and the remaining 15 are reported here for the first time, noting that one dwarf (dw1317-4255) has recently been confirmed to be a true member of the Centaurus A group Crnojević et al. 2018). The set of zoom-in images in Figure 1 show the dwarf candidates and measure $2'$ on a side, corresponding to physical $\sim 2.2 \times 2.2$ kpc² regions at the distance of NGC 5128. We point out that by employing a “by eye” detection technique, we are unable to make a robust estimate of the completeness limit to our imaging in a straightforward manner and thus cannot make broad statements on the true total population of dwarfs in this region. We instead defer such an analysis to a future work detailing the overall properties of dwarfs detected throughout our survey region, noting that a lack of completeness estimate does not affect our conclusions.

We use GALFIT (v3.0.5; Peng et al. 2010) to measure the structural and photometric properties of the dwarfs. We first create $3'.65 \times 3'.65$ (4×4 kpc²) image cutouts in all filters centered on each dwarf. We model the dwarfs using 1D Sérsic (Sérsic 1963) profiles defined as $I(r) = I_{\text{eff}} \exp\{-b_n[(r/r_{\text{eff}})^{1/n} - 1]\}$,

described by effective radius r_{eff} , the intensity I_{eff} at r_{eff} , and parameters defining the model shape n and b_n that are linked such that half of the total model light is contained within r_{eff} .

For each band we use an iterative surface-brightness (μ) model-fitting approach (Muñoz et al. 2015; Eigenthaler et al. 2018; Ordenes-Briceño et al. 2018a) by starting with reasonable initial guesses for magnitudes and sizes, and run SE on each cutout with a low detection threshold (DETECT_THRESH = 0.5) to construct a segmentation map to mask non-dwarf sources. We then run GALFIT on the masked image and allow all of the parameters—including the minor-to-major iso-photical axis ratio (b/a) and position angles (PAs)—to vary simultaneously. In most cases, models quickly converge to a solution, and in the cases that fail we fix the input magnitude and r_{eff} to obtain reasonable estimates on b/a and n , and then fix those parameters while freeing the magnitudes and sizes for refinement. Once an initial model solution has been derived, we then subtract it from the original image, use SE to derive an improved mask and generate a more refined dwarf model, and iterate this process until dwarf properties negligibly vary.

The results of this technique are shown in Figure 2 for a selection of dwarfs, where each block is titled by the dwarf identifiers. In each block, the original monochromatic imaging is shown in the upper rows with the corresponding models in the middle rows above the residual images. Close inspection of the residuals shows that the models estimate the μ profiles very well, with the iterative masking strategy effectively decoupling the dwarf signal even in the presence of foreground star contamination.

We list the full suite of photometric measurements in Table 1 alongside absolute V -band magnitudes (M_V), r_{eff} , n , and stellar mass estimates (M_* ; see Section 3.2). In all cases, the recovered photometric centroids for the dwarf candidates agree to $< 1''$ across filters, providing consistent anchors upon which the remaining model parameters are based. Total apparent magnitudes fall in the range $22.31 \gtrsim m_{u'}/\text{mag} \gtrsim 18.82$ and $19.97 \gtrsim m_{z'}/\text{mag} \gtrsim 16.40$ in the bluest and reddest filters, corresponding to foreground extinction-corrected (Schlafly & Finkbeiner 2011) $-7.42 \gtrsim M_V/\text{mag} \gtrsim -10.82$, using the conversion of Jester et al. (2005). Overall we find filter-dependent shape parameters in the range $0.15 \leq n \leq 2.73$, and $0.27 \leq b/a \leq 1.00$. Averaging across filters for each dwarf gives shape parameter ranges of $0.37 \leq n \leq 2.14$, and $0.47 \leq b/a \leq 0.89$ with a sample average $\langle n \rangle \approx 0.94$ and $\langle b/a \rangle \approx 0.72$, consistent with typical structural parameters of other dwarf galaxies in the nearby universe (e.g., Eigenthaler et al. 2018).

While GALFIT is excellent for model fitting, it is deficient in error estimation. For this, we use the ensemble of all five filters to place uncertainty estimates on the overall sizes and magnitudes. Table 1 lists the mean of each set of filter-dependent model r_{eff} along with corresponding 1σ error budgets. To estimate errors on the total dwarf magnitudes we use the variance in the sets of modeled r_{eff} , n , and b/a to generate new models by fixing each at their maximized/minimized values, and leaving the magnitudes unconstrained. We use the resulting sets of six models to determine the set of (r_{eff} , n , b/a) that produces the brightest/faintest magnitudes and adopt the difference as the uncertainties listed in Table 1.

3.2. Dwarf Stellar Masses

We compute M_* by fitting the extinction-corrected total dwarf magnitudes to SEDs predicted by simple stellar

⁵ <http://www.astromatic.net/>

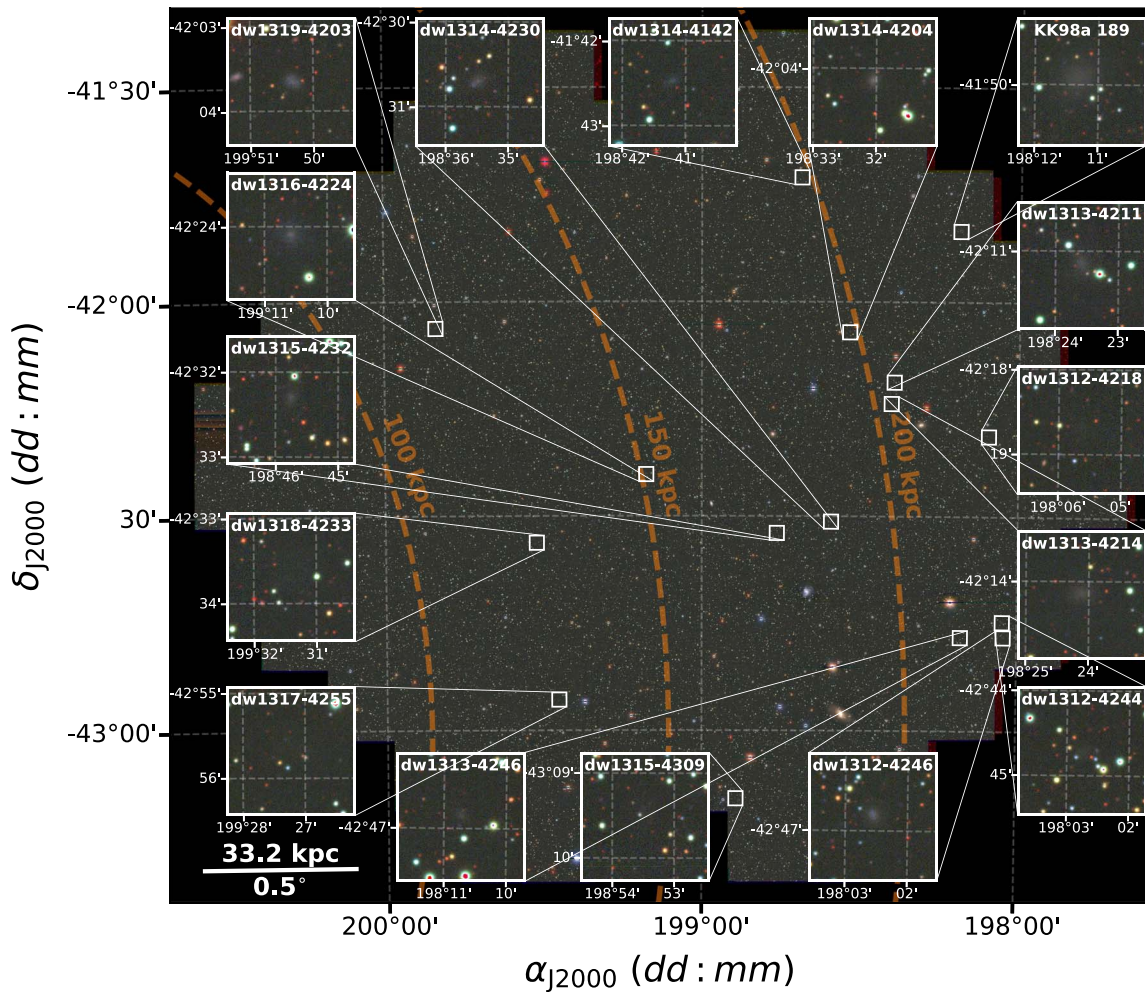


Figure 1. Locations of the new dwarf galaxy candidates on a $u'g'z'$ -based RGB color image. White-bordered images show $1/5 \times 1/5$ cutouts centered on the dwarfs, corresponding to $\sim 1.7 \times 1.7 \text{ kpc}^2$ at the distance of NGC 5128. The scale of the background frame is indicated in the lower-left corner. Dashed orange curves show distances corresponding to 100, 150, and 200 kpc from NGC 5128. North is up, east is to the left.

population (SSP) synthesis models (Bruzual & Charlot 2003). We allow SSP ages and metallicities in the ranges 1–15 Gyr and 0.0001–0.05 [Z/H]. We calculate the χ^2 goodness of fit for masses predicted between our observed photometric SEDs, and all SSP models. We assume an average \mathcal{M}_* , weighted by $\exp(-\chi^2)$, which together with the allowed ranges in age/metallicity help to mitigate the age–metallicity degeneracy (Zhang et al. 2017). The resulting \mathcal{M}_* estimates are listed in the last column of Table 1, and we find that they occupy a relatively narrow range of $5.17 \lesssim \log \mathcal{M}_*/M_\odot \lesssim 6.48$, with a mean $\log \langle \mathcal{M}_*/M_\odot \rangle = 5.73$. With sizes of $70 \lesssim r_{\text{eff}}/\text{pc} \lesssim 300$, these objects are broadly consistent with properties of LG dSphs, in particular those that show the highest stellar surface densities, and have many analogs in the Local Volume (LV; Chiboucas et al. 2009; McConnachie 2012; Müller et al. 2015, 2017a, see also Figure 3).

3.3. Size–Luminosity Relation

Figure 3 compares the modeled r_{eff} and total luminosities to other low-mass stellar systems in the NGC 5128–M83 complex (Crnojević et al. 2014, 2016; Müller et al. 2015, 2017a), and for additional context to various other dwarfs in the LV, including the M81, M101, M96, and Leo systems (Chiboucas et al. 2009; Merritt et al. 2014; Javanmardi et al. 2016; Bennet et al. 2017;

Henkel et al. 2017; Müller et al. 2017b, 2018a; Park et al. 2017), and the Fornax galaxy cluster core (Muñoz et al. 2015; Eigenthaler et al. 2018). We also show low-mass satellites identified in the LG (McConnachie 2012; Bechtol et al. 2015; Smercina et al. 2017; Homma et al. 2018; Muñoz et al. 2018b). For consistency with the LG dwarf data, where possible we show absolute V -band magnitudes converted from g' - and r' -band magnitudes (Jester et al. 2005); however, for some of the dwarfs (Chiboucas et al. 2009; Crnojević et al. 2016; Eigenthaler et al. 2018) neither g' nor r' imaging is available, so we defer to those that are available.

The size–luminosity relation of the new candidates shows a similar slope as other low-luminosity dwarfs in the nearby universe. Our selection technique biases us toward higher μ_V such that the new candidates fall almost parallel to lines of iso- μ_V (gray dashed lines), a trend that is not replicated by LG systems. The faintest of the new dwarfs populate a parameter space mostly devoid of LG analogs, but with several representative systems found throughout the LV. We note that four candidates—namely T18-dw1312-4247, 1314-4204, 1314-4231, and 1319-4203—fall below the main $r_{\text{eff}}-M_V$ relation with $r_{\text{eff}} \simeq 100 \text{ kpc}$ and $M_V \simeq -9 \text{ mag}$. These objects have no known analogs and we thus consider the possibility of them being associated with background galaxies at a distance of $\sim 50 \text{ Mpc}$. Should this be the case, we indicate the

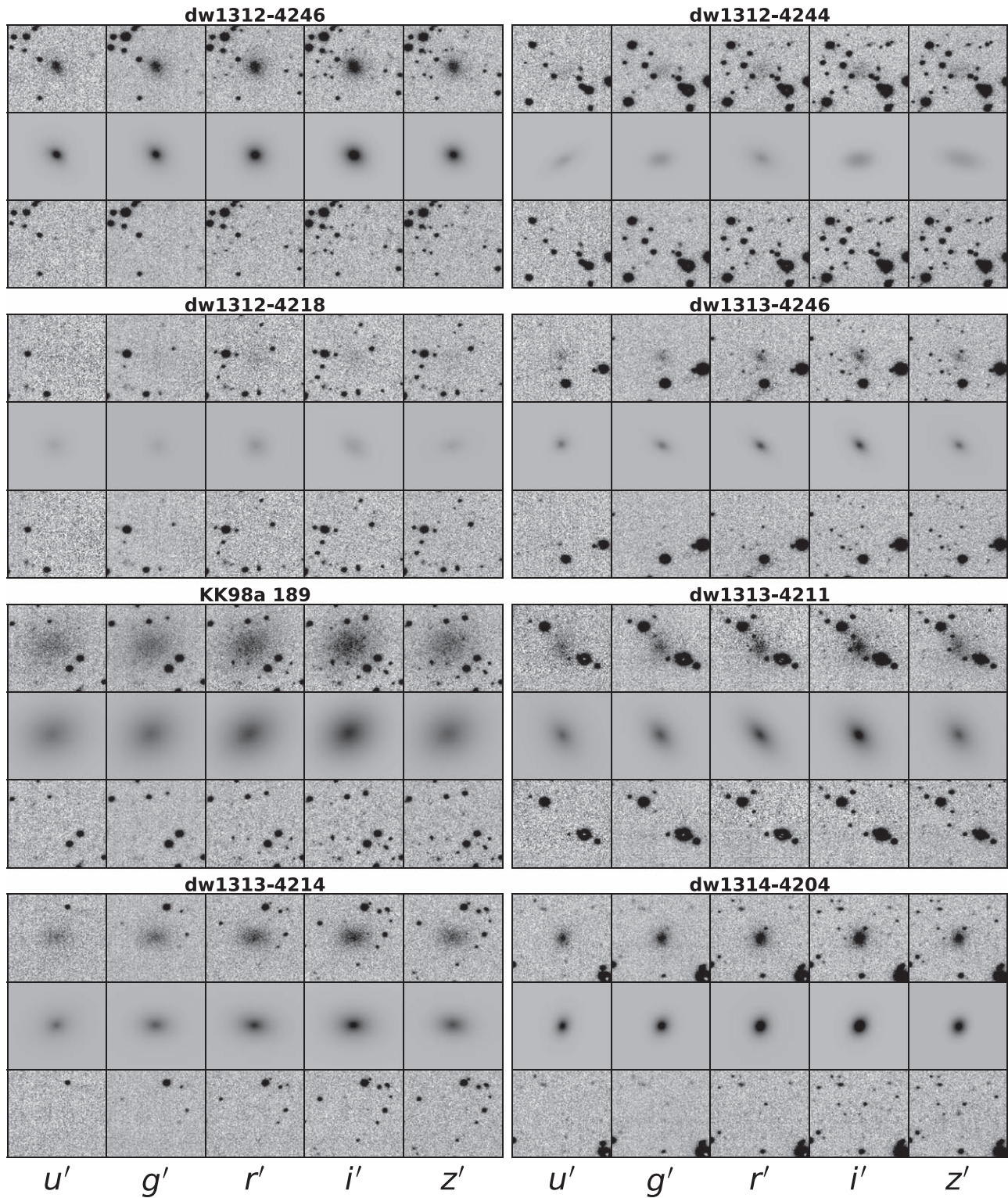


Figure 2. Sample of dwarf galaxy model fits. Blocks are titled by the dwarf identifiers, and show results in the $u'g'r'i'z'$ filters from left to right. All images measure $\sim 55''$ ($\sim 1 \text{ kpc}^2$) on a side. Upper rows in each block show original imaging, with the GALFIT models in the central rows, and model-subtracted residual frames in the row below.

size–luminosity parameter locations for the whole sample by dashed star symbols. We discuss this notion further in Section 4, where we find them more likely to be associated with NGC 5128.

Many of the new candidates coincide with the faintest dwarf galaxies known in the Fornax galaxy cluster at $M_V \simeq -8 \text{ mag}$

(Eigenthaler et al. 2018), and overlap with several dwarf galaxies elsewhere in the LV; however, a sharp truncation in the size–luminosity relation is seen beyond the faintest dwarf candidates, with a noticeable gap near $-7.5 \lesssim M_V/\text{mag} \lesssim -5.5$. We refrain from speculating on the dearth of LG dwarfs in this region, but note that such compact dwarfs beyond the LG can exhibit similar

Table 1
Photometric Properties of the Dwarf Galaxy Candidates

ID	α_{J2000} (hh: mm: ss)	δ_{J2000} (dd: mm: ss)	u' (mag)	g' (mag)	r' (mag)	i' (mag)	z' (mag)	M_V (mag)	r_{eff} ($''$)	n	$\log \mathcal{M}_*$ (M_\odot)
dw1312-4246	13:12:10.18	-42:46:48.53	20.27 \pm 0.11	18.76 \pm 0.12	18.81 \pm 0.17	17.76 \pm 0.19	17.86 \pm 0.13	-9.37	6.23 \pm 0.70	1.32 \pm 0.35	5.89 ^{+0.34} _{-0.36}
dw1312-4244	13:12:10.93	-42:44:43.66	21.90 \pm 0.26	20.26 \pm 0.19	19.88 \pm 0.12	19.18 \pm 0.33	18.75 \pm 0.47	-8.12	7.51 \pm 1.32	0.68 \pm 0.24	5.35 ^{+0.35} _{-0.38}
dw1312-4218	13:12:22.48	-42:18:41.58	21.98 \pm 0.18	21.23 \pm 0.24	20.16 \pm 0.13	19.58 \pm 0.12	19.97 \pm 0.15	-7.54	6.39 \pm 0.66	0.68 \pm 0.07	5.17 ^{+0.34} _{-0.35}
dw1313-4246	13:12:42.87	-42:46:50.57	21.76 \pm 0.11	20.32 \pm 0.12	20.11 \pm 0.13	19.02 \pm 0.13	18.92 \pm 0.11	-7.95	5.39 \pm 0.65	1.32 \pm 0.19	5.43 ^{+0.35} _{-0.49}
dw1313-4211	13:13:34.28	-42:11:08.38	19.74 \pm 0.09	18.49 \pm 0.08	18.29 \pm 0.07	17.13 \pm 0.08	17.14 \pm 0.09	-9.79	12.00 \pm 0.96	1.07 \pm 0.11	6.15 ^{+0.35} _{-0.44}
dw1313-4214	13:13:36.40	-42:14:08.11	20.11 \pm 0.12	18.78 \pm 0.16	18.43 \pm 0.15	17.31 \pm 0.16	17.61 \pm 0.17	-9.58	9.69 \pm 1.19	1.06 \pm 0.20	6.03 ^{+0.35} _{-0.40}
dw1314-4204	13:14:08.17	-42:04:08.51	20.78 \pm 0.05	19.18 \pm 0.05	18.97 \pm 0.05	18.06 \pm 0.05	18.22 \pm 0.04	-9.11	4.47 \pm 0.30	0.91 \pm 0.14	5.78 ^{+0.35} _{-0.35}
dw1314-4230	13:14:21.93	-42:30:41.87	20.96 \pm 0.20	19.35 \pm 0.12	19.05 \pm 0.16	18.07 \pm 0.09	17.86 \pm 0.11	-8.96	5.92 \pm 0.72	0.89 \pm 0.28	5.89 ^{+0.35} _{-0.56}
dw1314-4142	13:14:44.82	-41:42:28.27	21.62 \pm 0.09	20.30 \pm 0.07	20.55 \pm 0.04	19.44 \pm 0.04	19.79 \pm 0.08	-7.74	3.89 \pm 0.25	1.01 \pm 0.40	5.23 ^{+0.35} _{-0.30}
dw1315-4232	13:15:02.98	-42:32:17.78	20.88 \pm 0.21	19.58 \pm 0.23	19.02 \pm 0.14	18.02 \pm 0.18	18.32 \pm 0.21	-8.91	8.44 \pm 1.78	1.50 \pm 0.37	5.76 ^{+0.35} _{-0.42}
dw1315-4309	13:15:33.97	-43:09:27.18	22.31 \pm 0.12	21.17 \pm 0.18	20.63 \pm 0.18	19.51 \pm 0.15	19.31 \pm 0.17	-7.42	6.05 \pm 0.76	0.46 \pm 0.14	5.27 ^{+0.36} _{-0.51}
dw1316-4224	13:16:42.27	-42:24:05.32	19.34 \pm 0.22	17.77 \pm 0.15	17.94 \pm 0.25	16.86 \pm 0.20	16.84 \pm 0.14	-10.32	14.34 \pm 2.01	2.14 \pm 0.58	6.30 ^{+0.34} _{-0.35}
dw1317-4255	13:17:48.49	-42:55:40.45	21.54 \pm 0.22	19.70 \pm 0.21	19.89 \pm 0.17	18.61 \pm 0.25	18.73 \pm 0.30	-8.46	12.93 \pm 1.11	0.37 \pm 0.09	5.55 ^{+0.35} _{-0.31}
dw1318-4233	13:18:05.59	-42:33:37.10	20.67 \pm 0.57	19.47 \pm 0.42	18.84 \pm 0.46	18.41 \pm 0.38	18.82 \pm 0.34	-9.14	16.78 \pm 3.95	0.37 \pm 0.13	5.61 ^{+0.32} _{-0.42}
dw1319-4203	13:19:21.26	-42:03:38.74	20.47 \pm 0.05	19.12 \pm 0.06	19.05 \pm 0.08	18.11 \pm 0.04	18.11 \pm 0.07	-9.15	4.91 \pm 0.40	0.52 \pm 0.09	5.82 ^{+0.34} _{-0.34}
KK98a 189	13:12:45.23	-41:49:55.23	18.82 \pm 0.08	17.40 \pm 0.04	17.35 \pm 0.04	16.42 \pm 0.03	16.40 \pm 0.04	-10.82	14.94 \pm 0.68	0.73 \pm 0.05	6.48 ^{+0.35} _{-0.33}

Note. Column (1) lists dwarf identifiers based on the on-sky coordinates listed in columns (2)–(3). Columns (4)–(8) show the total apparent magnitudes in each filter, followed by the foreground extinction-corrected absolute V -band luminosities, effective radii, average Sérsic index, and stellar mass estimates in columns (9), (10), (11), and (12), respectively.

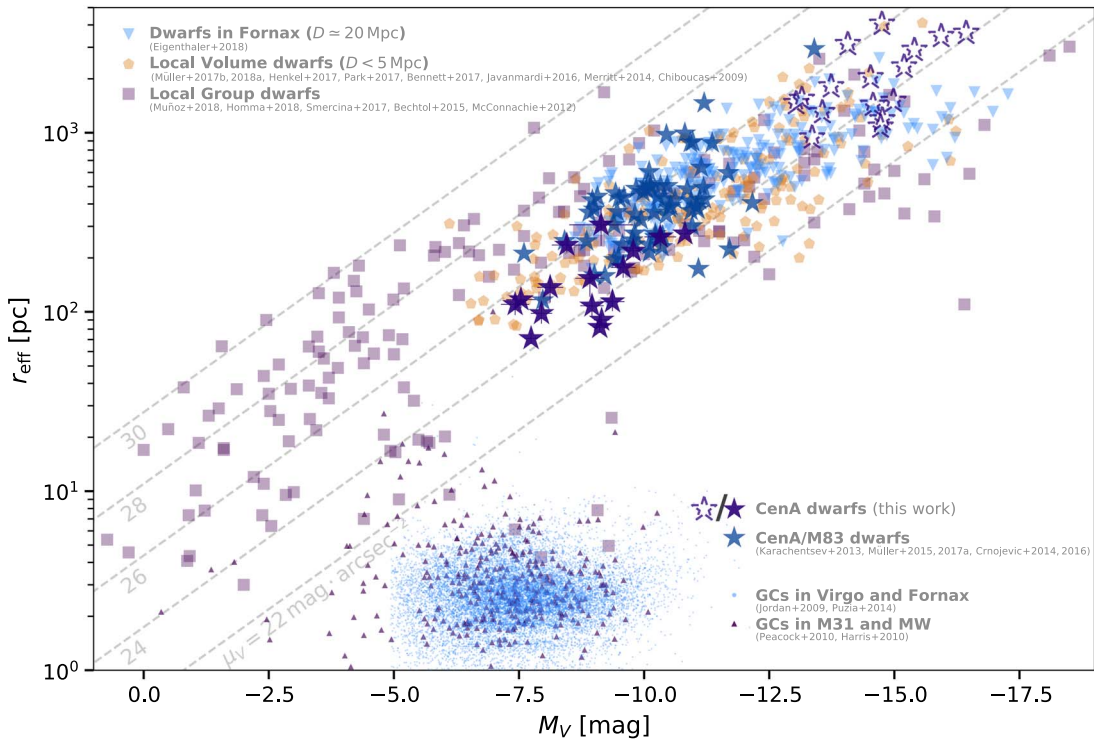


Figure 3. Size–luminosity diagram including the present dwarf candidates, LG ultra-faint dwarfs and dSphs, and other dwarf galaxies within the LV and nearby universe, including Fornax cluster dwarfs, and dwarf galaxies associated with more isolated nearby ($\lesssim 50$ Mpc; see Section 3.3) giant galaxies. We differentiate those already known in the Centaurus A/M83 complex for easier comparison to the candidates presented in this Letter (purple vs. blue stars). Where available, we plot V -band luminosities and convert g' and r' magnitudes to V using the relation of Jester et al. (2005); if this is not possible, we plot g' or r' -band photometry as available from the literature. Empty dashed stars show the sample from this Letter shifted to the distance of a background group at a distance of 50 Mpc (see Section 4).

morphologies to background elliptical galaxies in monochromatic imaging, and only reveal themselves via RGB imaging with sufficiently wide SED coverage. Given this and the overall difficulty identifying such objects beyond the Local Group, it is likely that this region will continue to be filled out as future imaging campaigns probe ever deeper into various giant galaxy environments.

3.4. Comparison to Stellar Population Synthesis Predictions

Figure 4 shows a comparison of the new dwarf candidates to those in the Fornax galaxy cluster with u' , g' , and i' imaging (Muñoz et al. 2015; Eigenthaler et al. 2018), with the same symbol/color definitions as in Figure 3. We also plot nuclear star clusters (NSCs) corresponding to the nucleated dwarf galaxies present in the Fornax sample (orange; Ordenes-Briceño et al. 2018b), and compact stellar systems (CSSs) including GCs and ultra-compact dwarf galaxies (UCDs) also confirmed to be members of the Fornax cluster (brown; Wittmann et al. 2016). Finally, we also show for comparison a large sample of NGC 5128 GCs (red points; Taylor et al. 2017).

The left column shows $(u' - i')_0$, $(u' - g')_0$, and $(g' - i')_0$ versus $M_{g'}$ color–magnitude diagrams (CMDs) for the various samples. The trend toward bluer colors at fainter luminosities is apparent for the Fornax dwarfs in all three panels, most prominently for the $(u' - i')_0$ CMD, and is typically considered to represent a mass–metallicity relation. The new NGC 5128 dwarf candidates are offset from the Fornax dwarf sample toward redder average colors by $\Delta(u' - i')_0 \approx 0.6$ and $\Delta(g' - i')_0 \approx 0.4$ mag, and appear more consistent—in terms

of stellar population properties—with the nuclei and CSS populations, despite having much more diffuse morphologies.

The right-hand column in Figure 4 shows a comparison of the sample color distributions, indicated by the shaded histograms aligned to the y-axes, and corresponding Epanechnikov-kernel density estimates (thicker solid lines). We find that while there is some overlap with the generally older and metal-poor Fornax dwarf galaxies, the bulk of the NGC 5128 dwarfs have colors consistent with the secondary red peaks shown by the CSS samples, which shows up most prominently in the $(u' - i')_0$ color. If the redder colors exhibited by the NGC 5128 dwarfs are due to a metallicity effect, then this might imply early formation within the halos of the giant galaxy progenitors of NGC 5128 itself, where they could incorporate material rapidly enriched by the giants at early times. Alternatively, higher metallicities could be due to either a prolonged primordial star formation history enabling self-enrichment, or a non-primordial burst of star formation may have occurred, possibly by previously enriched gas shocked upon infall into NGC 5128’s halo. The former scenario might be expected from the density-morphology relation (Dressler 1980), where early star formation failed to be suppressed owing to the relatively low-density environment of the Centaurus A group precluding a high number of harassing encounters. In either case, it would require that these dwarfs must have at one point been embedded in dark matter halos of sufficient mass to retain enriched material expelled by early supernovae, which was likely subsequently stripped during infall, thus preventing very recent star formation that would give rise to bluer colors.

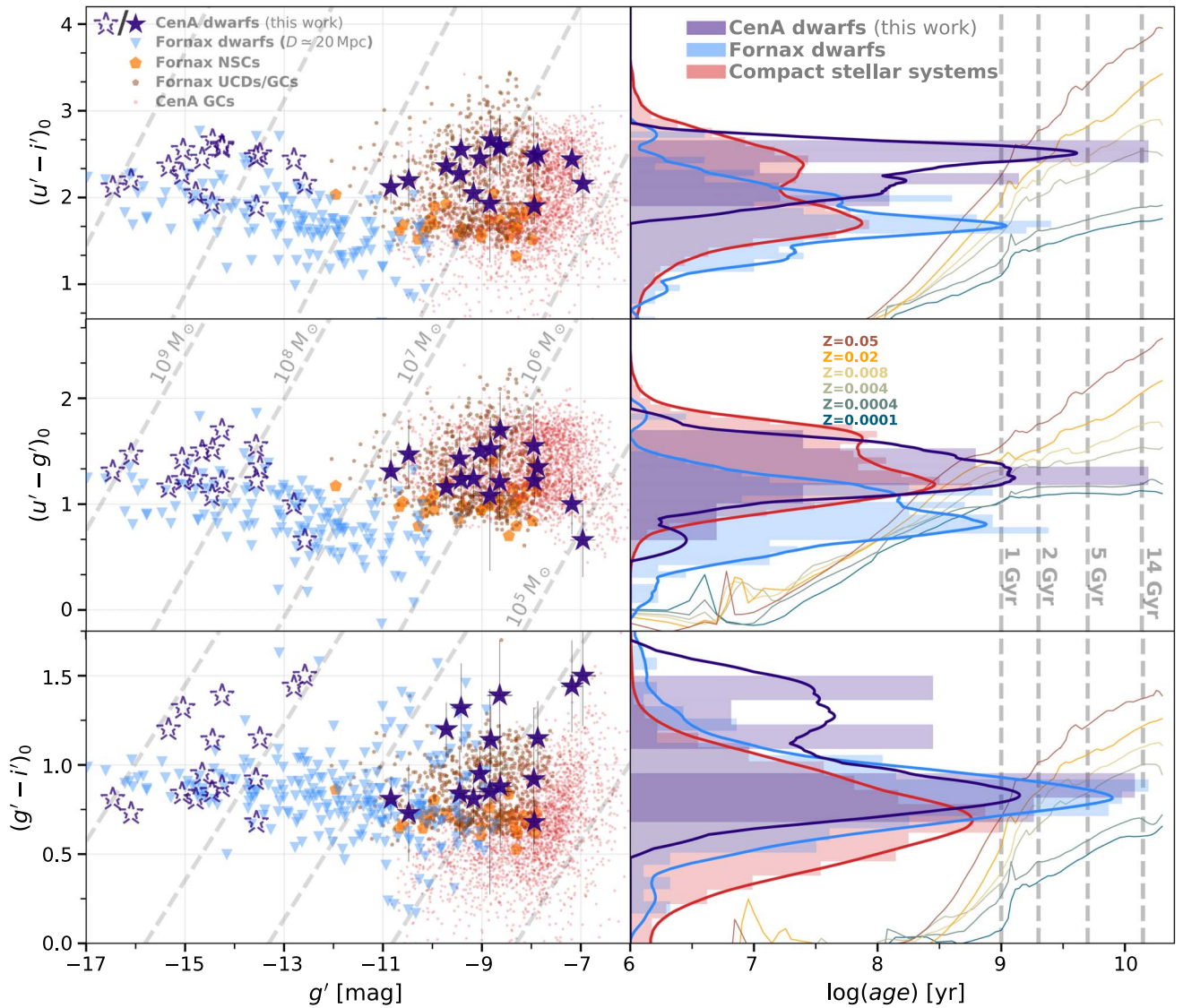


Figure 4. Photometric color properties of low-mass stellar systems. Left panels: $(u' - i')_0$, $(u' - g')_0$, and $(g' - i')_0$ vs. g' color–magnitude diagrams are shown from top to bottom, where the current sample is compared to the Fornax cluster sample shown in Figure 3 (blue triangles), where respective photometry is available. Purple stars show the new NGC 5128 dwarfs, and dashed gray lines show iso- M_* relations using the prescription of Bell et al. (2003). Also shown by orange and brown points are color information for Fornax cluster CSSs including NSCs, UCDS, and GCs, with red points representing NGC 5128 GCs. Right panels: color distributions are shown aligned along the y-axis for the Fornax (blue), NGC 5128 (purple), and combined CSS (red) samples and compared to Bruzual & Charlot (2003) SSP models for a range of metallicities shown by the colored tracks. SSP model tracks are indicated by the thin curves colored according to metallicity, with model ages corresponding to the logarithmic x-axis, and solid gray lines indicating 1, 2, 5, and 14 Gyr.

4. Discussion and Summary

We have increased the population of likely dwarf galaxy satellites of the Centaurus A group by 15, and recovered a single known dwarf (Karachentseva & Karachentsev 1998; Karachentsev et al. 2013) in the five optical $u'g'r'i'z'$ bands. All candidates reside ~ 100 – 225 kpc in NGC 5128’s northwest halo, and their relatively small sizes ($r_{\text{eff}} \approx 70$ – 300 pc) and stellar masses ($M_* \approx 10^5$ – $6 M_\odot$) are mostly similar to dSphs found in the Local Universe; however, their relatively high $\mu_{\text{eff}} \approx 23$ – 26 mag arcsec $^{-2}$ partially populate a region of the low-mass size–luminosity relation not seen in the LG. Rather, these dwarf galaxies appear to be a natural extension of the size–luminosity relation seen in larger galaxy complexes in the nearby universe toward fainter magnitudes that are not yet well sampled in these complexes.

The relatively high μ_V may indicate that, rather than being members of the Centaurus A group, these candidates may be associated with known giant galaxies in the background. To guard against this, we queried the NASA/IPAC Extragalactic Database for any background sources classified as galaxies falling within $30'$ of a given dwarf candidate that have measured redshifts and/or distances. This projected radius corresponds to a physical separation of ~ 200 kpc from a giant host located 25 Mpc away—close enough that dwarf galaxies would be easily spotted by their diffuse natures, while orbiting within a purported host-centric radius where the projected surface number density profile remains high (e.g., Ordenes-Briceño et al. 2018a). Through this exercise, we cannot formally exclude the possibility that at least some of these galaxies, particularly those lying in the southwestern region of the imaging, may be associated with the galaxy group NGC 5011, located at a distance of ~ 50 Mpc.

Given this potential host, we calculate the corresponding sizes and luminosities of our candidates should they indeed be members of NGC 5011. We plot the results on Figures 3 and 4 as empty dashed stars, and find that, while the faintest half of our candidates fall within the locus of known dwarf galaxies at the bright/large end of the size–luminosity relation, the brightest show a combination of size and luminosity that is essentially devoid of analogs in the LV.

When we apply the same exercise to the CMDs in Figure 4, we find that this implies luminosities that are similar to the brightest dwarf galaxies reported in the Fornax sample, but such luminous dwarf galaxies are simply not found in other LV galaxy complexes that are—like NGC 5128—significantly less massive hosts than Fornax. Moreover, if a significant number of these candidates are in fact associated with NGC 5011, this would imply a very shallow slope for the NGC 5011 faint-end galaxy luminosity function. We cannot formally exclude this possibility, given the implication that a group like NGC 5011 would be hosting a significant population of luminous dwarfs thus far only found in galaxy cluster environments. This therefore suggests that it is likely that most, if not all, of the present candidates are indeed associated with NGC 5128, which will ultimately require spectroscopic verification.

Given that the majority of new dwarf candidates are very likely to be associated with NGC 5128, we turn our attention back to Figure 1, specifically noting the existence of at least two groups of three galaxies (dw1314-4204, 1313-4211, and 1313-4214; and dw1312-4244, 1312-4246, and 1313-4246), each with projected separations of $\lesssim 20$ kpc. While it is impossible to determine their true 3D locations in NGC 5128’s halo with the current data, we note that such groups are to be expected from modern cosmological zoom-in simulations (e.g., Wetzel et al. 2015; Besla et al. 2018), and thus may represent important examples of dwarf groups in the early stages of interaction while infalling upon NGC 5128’s halo. If so, then these groups, and the present dwarf sample as a whole may represent a valuable opportunity to study these processes in detail in the very nearby universe.

We thank the anonymous referee for a fair critique of this work, and the useful feedback that served to improve the original manuscript.

M.A.T. is supported by the Gemini Observatory, which is operated by the Association of Universities for Research in Astronomy, Inc., on behalf of the international Gemini partnership of Argentina, Brazil, Canada, Chile, and the United States of America. This project is supported by FONDECYT Regular project No. 1161817 and the BASAL Center for Astrophysics and Associated Technologies (PFB-06).






This project used data obtained with the Dark Energy Camera (DECam), which was constructed by the Dark Energy Survey (DES) collaboration.

This research has made use of the NASA Astrophysics Data System Bibliographic Services, the NASA Extragalactic Database, and the SIMBAD database and VizieR catalog access tool, operated at CDS, Strasbourg, France (Wenger et al. 2000).

Facility: CTIO:Blanco/DECam.

software: ASTROPY (Astropy Collaboration et al. 2013), MATPLOTLIB (Hunter 2007), SCAMP (Bertin et al. 2002), SWARP (Bertin 2006), SOURCE EXTRACTOR (Bertin & Arnouts 1996), GALFIT (Peng et al. 2010),

ORCID iDs

Matthew A. Taylor  <https://orcid.org/0000-0003-3009-4928>
 Paul Eigenthaler  <https://orcid.org/0000-0001-8654-0101>
 Thomas H. Puzia  <https://orcid.org/0000-0003-0350-7061>
 Roberto P. Muñoz  <https://orcid.org/0000-0003-1743-0456>
 Yasna Ordenes-Briceño  <https://orcid.org/0000-0001-7966-7606>

References

- Astropy Collaboration, Robitaille, T. P., Tollerud, E. J., et al. 2013, *A&A*, **558**, A33
- Bechtol, K., Drlica-Wagner, A., Balbinot, E., et al. 2015, *ApJ*, **807**, 50
- Bell, E. F., McIntosh, D. H., Katz, N., & Weinberg, M. D. 2003, *ApJS*, **149**, 289
- Belokurov, V., Walker, M. G., Evans, N. W., et al. 2010, *ApJL*, **712**, L103
- Bennet, P., Sand, D. J., Crnojević, D., et al. 2017, *ApJ*, **850**, 109
- Bertin, E. 2006, in ASP Conf. Ser. 351, *Astronomical Data Analysis Software and Systems XV*, ed. C. Gabriel et al. (San Francisco, CA: ASP), 112
- Bertin, E., & Arnouts, S. 1996, *A&AS*, **117**, 393
- Bertin, E., Mellier, Y., Radovich, M., et al. 2002, in ASP Conf. Ser. 281, *Astronomical Data Analysis Software and Systems XI*, ed. D. A. Bohlender, D. Durand, & T. H. Handley (San Francisco, CA: ASP), 228
- Besla, G., Patton, D. R., Stierwalt, S., & Rodríguez-Gomez, V. 2018, *MNRAS*, **480**, 3376
- Bruzual, G., & Charlot, S. 2003, *MNRAS*, **344**, 1000
- Chiboucas, K., Karachentsev, I. D., & Tully, R. B. 2009, *AJ*, **137**, 3009
- Crnojević, D., Sand, D. J., Bennet, P. N., et al. 2018, arXiv:1809.05103
- Crnojević, D., Sand, D. J., Caldwell, N., et al. 2014, *ApJL*, **795**, L35
- Crnojević, D., Sand, D. J., Spekkens, K., et al. 2016, *ApJ*, **823**, 19
- Dressler, A. 1980, *ApJ*, **236**, 351
- Eigenthaler, P., Puzia, T. H., Taylor, M. A., et al. 2018, *ApJ*, **855**, 142
- Harris, G. L. H., Rejkuba, M., & Harris, W. E. 2010, *PASA*, **27**, 457
- Henkel, C., Javanmardi, B., Martínez-Delgado, D., Kroupa, P., & Teuwen, K. 2017, *A&A*, **603**, A18
- Homma, D., Chiba, M., Okamoto, S., et al. 2018, *PASJ*, **70**, S18
- Hunter, J. D. 2007, *CSE*, **9**, 90
- Ibata, R. A., Lewis, G. F., Conn, A. R., et al. 2013, *Natur*, **493**, 62
- Javanmardi, B., Martínez-Delgado, D., Kroupa, P., et al. 2016, *A&A*, **588**, A89
- Jester, S., Schneider, D. P., Richards, T. H., et al. 2005, *AJ*, **130**, 873
- Karachentsev, I. D., Makarov, D. I., & Kaisina, E. I. 2013, *AJ*, **145**, 101
- Karachentseva, V. E., & Karachentsev, I. D. 1998, *A&A*, **127**, 409
- McConnachie, A. W. 2012, *AJ*, **144**, 4
- Merritt, A., van Dokkum, P., & Abraham, R. 2014, *ApJL*, **787**, L37
- Müller, O., Jerjen, H., & Binggeli, B. 2015, *A&A*, **583**, A79
- Müller, O., Jerjen, H., & Binggeli, B. 2017a, *A&A*, **597**, A7
- Müller, O., Jerjen, H., & Binggeli, B. 2018a, arXiv:1802.08657
- Müller, O., Jerjen, H., Pawlowski, M. S., & Binggeli, B. 2016, *A&A*, **595**, A119
- Müller, O., Pawlowski, M. S., Jerjen, H., & Lelli, F. 2018b, *Sci*, **359**, 534
- Müller, O., Scalera, R., Binggeli, B., & Jerjen, H. 2017b, *A&A*, **602**, A119
- Muñoz, R. P., Eigenthaler, P., Puzia, T. H., et al. 2015, *ApJL*, **813**, L15
- Muñoz, R. R., Côté, P., Santana, F. A., et al. 2018a, *ApJ*, **860**, 65
- Muñoz, R. R., Côté, P., Santana, F. A., et al. 2018b, *ApJ*, **860**, 66
- Ordenes-Briceño, Y., Eigenthaler, P., Taylor, M. A., et al. 2018a, *ApJ*, **859**, 52
- Ordenes-Briceño, Y., Puzia, T. H., Eigenthaler, P., et al. 2018b, *ApJ*, **860**, 4
- Park, H. S., Moon, D.-S., Zaritsky, D., et al. 2017, *ApJ*, **848**, 19
- Pawlowski, M. S., Pflamm-Altenburg, J., & Kroupa, P. 2012, *MNRAS*, **423**, 1109
- Peng, C. Y., Ho, L. C., Impey, C. D., & Rix, H.-W. 2010, *AJ*, **139**, 2097
- Sánchez-Janssen, R., Ferrarese, L., MacArthur, L. A., et al. 2016, *ApJ*, **820**, 69
- Schlafly, E. F., & Finkbeiner, D. P. 2011, *ApJ*, **737**, 103
- Sérsic, J. L. 1963, *BAA*, **6**, 41
- Smercina, A., Bell, E. F., Slater, C. T., et al. 2017, *ApJL*, **843**, L6
- Taylor, M. A., Puzia, T. H., Muñoz, R. P., et al. 2017, *MNRAS*, **469**, 3444
- Valdes, F., Gruendl, R. & DES Project 2014, in ASP Conf. Ser. 485, *Astronomical Data Analysis Software and Systems XXIII*, ed. N. Manset & P. Forshay (San Francisco, CA: ASP), 379
- Wenger, M., Ochsenbein, F., Egret, D., et al. 2000, *A&AS*, **143**, 9
- Wetzel, A. R., Deason, A. J., & Garrison-Kimmel, S. 2015, *ApJ*, **807**, 49
- Wittmann, C., Lisker, T., Pasquali, A., Hilker, M., & Grebel, E. K. 2016, *MNRAS*, **459**, 4450
- Zhang, H.-X., Puzia, T. H., & Weisz, D. R. 2017, *ApJS*, **233**, 13